Non-Franck–Condon transitions in resonant autoionization of N_2O

Tomas Baer,[a) d)] Paul-Marie Guyon,[a)] Irene Nenner,[b)] Abdallah Tabché-Fouhaillé,[b)] René Botter,[b)] Luis F. A. Ferreira,[a)] and Thomas R. Govers[c)]

LURE, Laboratoire C.N.R.S., Université Paris-Sud, 91405 Orsay, France
(Received 8 September 1978)

Autoionization of N_2O between 12.89 and 16.4 eV was investigated by photoionization using the pulsed synchrotron radiation from ACO, Orsay's storage ring. Measurements were performed of threshold photoelectron spectra, photoionization spectra, and of photoelectron energy spectra. The latter were obtained from photoelectron time of flight distributions at selected wavelengths. The results suggest that autoionization in the Franck–Condon gap between the $\tilde{X}\,^2\Pi$ and the $\tilde{A}\,^2\Sigma^+$ states of N_2O^+ proceeds via two distinct mechanisms. The major autoionization process ($\approx$90%) produces the $\tilde{X}\,^2\Pi$ state in its low vibrational levels, while a resonant autoionization path ($\approx$10%) produces vibrationally excited $\tilde{X}\,^2\Pi$ ions. The latter process is associated with the production of low energy electrons with a distribution peaking sharply at zero energy. This resonant autoionization process appears to be a general phenomena for polyatomic molecules.

I. INTRODUCTION

The excitation of a low-lying electron into a Rydberg orbital can result in the formation of an autoionizing (or preionizing) state. The process of autoionization involves the transfer of energy from the ion core to the Rydberg electron which is ejected into the continuum. In molecules, the core can lose electronic, vibrational, or rotational energy, in which case we speak of electronically, vibrationally or rotationally induced autoionization. In electronically induced autoionization, both electronic and vibrational energy of the core can be transferred to the departing electron. Bardsley[1] and Smith[2,3] have derived expressions predicting the branching ratios to the final ionic states using the configuration interaction (CI) theory of Fano.[4,5] The assumption of the Born–Oppenheimer approximation in which the wave functions are products of vibrational and electronic wave functions leads to autoionization rates which are products of electronic transition probabilities and Franck–Condon factors between the neutral autoionizing and the final ionic states. These ideas have been applied in the interpretation of photoelectron spectra (PES) obtained from autoionizing levels of O_2,[6] and N_2,[7] and generally good agreement was noted between the predicted and measured distributions of final ionic vibrational levels. However, it should be noted that there is considerable uncertainty in the assignment of the relevant autoionization states of O_2. More recently, Duzy and Berry[8] have investigated electronically induced autoionization in N_2 by a perturbation technique involving configuration interaction. These authors also suggest the appropriateness of using Franck–Condon factors in calculating branching ratios, a conclusion supported by the available experimental evidence, namely, photoelectron spectroscopy (PES) at selected photon energies of a variety of molecules.[9,10]

A related problem is the observation of fragment ion appearance potentials (A. P.). There are numerous dissociative photoionization processes, such as those yielding O^+ from N_2O [11] and CO_2,[12] SO^+ from SO_2,[13] HCO^+ from H_2CO,[14] $C_3H_3^+$ from CH_3CCH,[15] and $CH_2CH\ CH_2$ [16] whose onsets are observed at the thermodynamic threshold, even though these limits lie at energies within the Franck–Condon gap where the probability for forming excited molecular ions (as determined by 21.21 eV PES[17]) is vanishingly small and orders of magnitudes too small to explain the observed fragment intensities. As a result of these observations, it has become apparent during the past 10 years that molecular ions are formed in high vibrational states via autoionization, even in cases[15,16] where the autoionization structure is not characterized by sharp peaks.[14,16,18,19]

An ion which has a particularly large Franck–Condon gap region is N_2O^+ (Fig. 1). Photoelectron spectra[17] of the $\tilde{X}\,^2\Pi$ state $[\cdots(1\Pi)^4(7\sigma)^2(2\Pi)^3]$ and the first excited

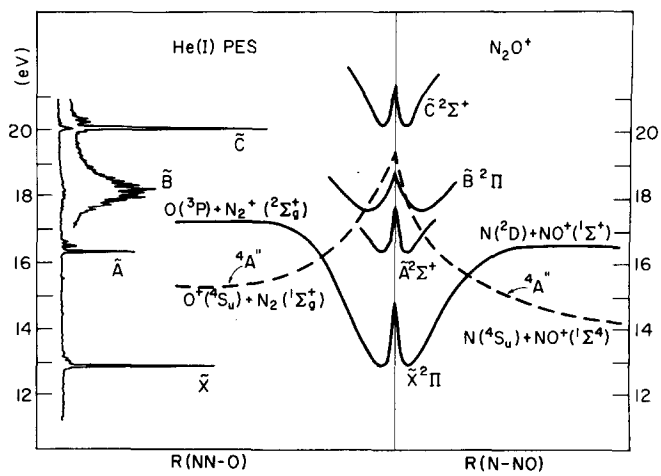

FIG. 1. Schematic potential diagrams of the electronic states of N_2O^+. The He(I) photoelectron spectrum is taken with permission from Ref. 17(a). The "$^4A''$" curve is estimated from the data of Ref. 25.

[a)]Laboratoire des Collisions Atomiques et Moléculaires, Bât. 351, Université Paris-Sud, 91405 Orsay, France.
[b)]DRA–SRIRMa, CEN Saclay, BP N° 2, 91190 Gif sur Yvette, France.
[c)]Laboratoire de Résonance Electronique et Ionique, Bât. 350, Université Paris-Sud, 91405 Orsay, France.
[d)]J. S. Guggenheim Fellow 1976–77, on leave from University of North Carolina, Chapel Hill, NC.

 0021-9606/79/041585-08$01.00

$\tilde{A}\,^2\Sigma^+$ state $[\cdots(1\Pi)^4(7\sigma)^1(2\Pi)^4]$ at 16.388 eV exhibit strong $v=0$ bands indicating that both ion states are linear as is the N_2O molecular ground state $\tilde{X}\,^1\Sigma^+$. Photoionization[11,20] and absorption[20,21] experiments have revealed strong autoionization structure in the region between the $\tilde{X}$ and $\tilde{A}$ states. Most of these peaks have been identified[11,20,21] as Rydberg states converging to the (0, 0, 0) and (0, 0, 1) vibrational levels of the $\tilde{A}\,^2\Sigma^+$ state. The most recent and complete analysis has been done by Berkowitz and Eland[11b] on the basis of photoionization mass spectra. The $\tilde{A}\,^2\Sigma^+$ state, which has been investigated by photoion–photoelectron coincidence, is predissociated.[22] However, this predissociation is slow and competes with $\tilde{A}\rightarrow\tilde{X}$ fluorescence.[23] This competition has been confirmed by photodissociation experiments.[24]

As evidenced by the He(I) PES of Fig. 1, the $\tilde{B}\,^2\Pi$ is characterized by a long and irregular progression of vibrational levels suggesting a significant change of geometry from the neutral ground state, $\tilde{X}\,^1\Sigma^+$. The $\tilde{C}\,^2\Sigma$ state is very likely linear and has equilibrium distances close to those of the $\tilde{X}$ and $\tilde{A}$ states.

The first two dissociation limits of N_2O^+ are $NO^+(^1\Sigma^+)$ + $N(^4S)$ at 14.19 eV and $O^+(^4S)+N_2(^1\Sigma^+)$ at 15.29 eV. Since neither the $\tilde{X}$ nor the $\tilde{A}$ states correlate to the observed fragment limits, it has been suggested that the $\tilde{A}\,^1\Sigma^+$ state was predissociated by an as yet unobserved repulsive $^4A''$ state which has recently been calculated in great detail by Hopper.[25] As shown in Fig. 1, this $^4A''$ state correlates to both dissociation products. The major electronic configuration of this quartet state is $\cdots(1\Pi)^4(7\sigma)^2(2\Pi)^2(3\Pi)^1$. The observation of the O^+ fragment at its thermochemical onset and of NO^+ within 0.7 eV of its dissociation limit, where no known ionic state of N_2O^+ can be formed by direct ionization, has been interpreted by Berkowitz and Eland[11b] as due to autoionization of Rydberg states directly to the repulsive $^4A''$ state of the ion.

In order to determine more directly the fate of autoionizing states, we undertook the investigation of autoionization in N_2O by combining several photoionization techniques. These were (a) threshold photoelectron spectroscopy (TPES); (b) photoionization mass spectrometry; (c) time of flight electron energy analysis; and (d) to a minor extent, photoion–photoelectron coincidence. Only (a), (b), and (c) will be described in some detail in the following section. The technique for the photoion–photoelectron coincidence experiment has been outlined briefly[26] and will be discussed further in a future paper.

II. EXPERIMENTAL

Synchrotron radiation from ACO,[27] Orsay's storage ring, dispersed by a 1.5 m Pouey monochromator with a 3600 lines/mm platinum coated holographic grating, was refocused at the center of the photoionization region where it crossed a jet of gas effusing from a fine hypodermic needle. The photon bandwidth was 0.5–1 Å and a maximum light flux of 10^9 photons/Å sec was obtained at about 550 Å. The photoionization region was mounted in a chamber pumped by a 400 l/sec Balzers-Pfeiffer turbomolecular pump. The pressure within the jet was about 50 times the background pressure of 5×10^{-5} Torr during experiments.

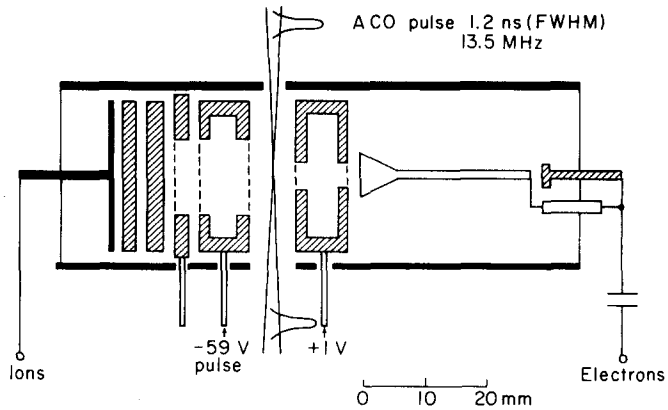

FIG. 2. Schematic of ionization chamber.

The photoionization region is shown in Fig. 2. The disposition of the electrodes allowed electrons and ions to be extracted in opposite directions, at right angles to the photon and gas beams. It was constructed of gold plated copper, and the distance between plates was designed to satisfy the space focusing conditions[28] for the ions as well as for the electrons. The time of flight (TOF) of charged particles having zero initial kinetic energy was thus independent of their initial position. A 90% transparent gold mesh covered the 4 mm and 12 mm diameter apertures on the electron and ion sides, respectively. Electrons were collected in the presence of a 1 V/cm electric field while for ion analysis the field was increased to 60 V/cm. The electrons were detected by a spiraltron and ions by a channel array detector.

A. Photoelectron spectra by electron time of flight analysis

The electron time of flight (TOF) distributions were measured by using the electron signal as start and the delayed light signal as stop inputs to a time to pulse height converter, the output of which was fed into a multichannel pulse height analyzer. To a first approximation photoelectrons are ejected isotropically, especially those of low energy. Those ejected perpendicular to the applied electric field hit the walls and apertures and are thus not detected. Those energetic electrons ejected along the field axis, either toward or away from the electron detector arrive earlier or later than nominally zero energy electrons. Examples of electron TOF distributions obtained by photoionizing Ar near the ionization threshold are shown in Fig. 3. Those electrons with initial energy greater than 0.5 eV which are ejected away from the electron detector enter the ion drift region and are lost. The electron TOF data for N_2O which involved the detection of electrons with up to 3.5 eV was limited to the electrons ejected toward the detector.

The characteristics of photoelectron spectra by electron TOF and the details of TOF → energy conversion are discussed elsewhere[10,29] in detail and will be only outlined here. The resolution is very good (10 meV) near threshold, but rapidly worsens with energy as E

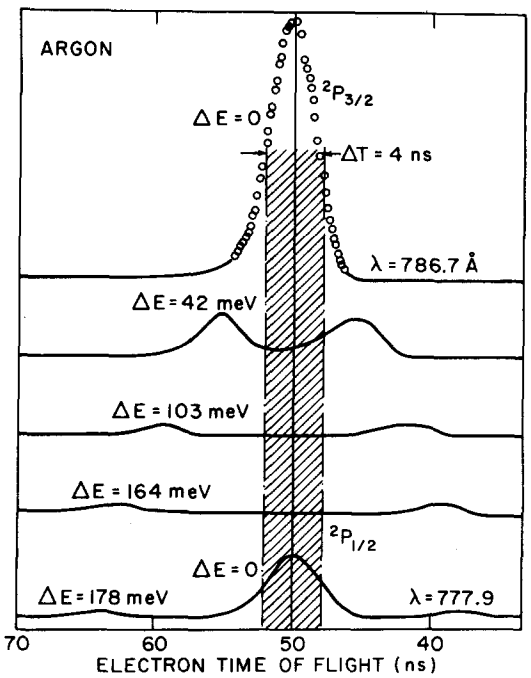

FIG. 3. Electron time of flight spectra of argon, taken at selected wavelengths from the $^2P_{3/2}$ threshold (786.7 Å) to the $^2P_{1/2}$ threshold (777.9 Å).

to the 1.5 power in the limit of high energy. The collection efficiency for electrons is a strong function of their energy.[30] This is illustrated in Fig. 3, where each electron TOF distribution is normalized to the same total number of ionization events. Therefore, the areas under the peaks directly give the relative collection efficiency for the electrons of the given energy. The raw electron TOF distributions were normalized with respect to this collection efficiency as well as the Jacobian dE/d (TOF) which converts the TOF to an energy scale. These two functions vary in opposite directions with the electron energy.

B. Threshold photoelectron spectra

The threshold photoelectron spectrum (TPES) is a scan of zero energy electrons versus photon energy. The TPES were obtained by gating the electron detector after each photon pulse with a time window centered on the arrival time of the zero energy electrons (Fig. 3). By operating in this manner we discriminate against hot electrons not only on the basis of their angular dispersion[30] but also on their temporal characteristics. Nearly all threshold electron experiments currently in use discriminate against energetic electrons by their angular dispersion.[31] However, in the absence of additional discrimination those electrons whose initial velocity vector is in the direction of the electron detector will be detected. These electrons have either been minimized and tolerated, or have been eliminated by dispersive analyzers[31d] at the cost of reduced collection efficiency. By our TOF discrimination, we lose no more than 40% of the true zero energy electrons while effectively eliminating energetic electrons with energies greater than 20 meV. The efficiency of the temporal discrimination of energetic electrons is illustrated in Fig. 4, which shows (a) the photoionization cross section of Ar near threshold obtained for a 1 Å monochromator band pass, (b) the TPES without temporal discrimination of "hot" electrons, and (c) the same TPES with a temporal gate of 4 nsec. The autoionized Rydberg structure which is still apparent though much reduced on curve *b* is now effectively suppressed. In the present setup, the collection efficiency for 1 eV electrons relative to zero energy electrons is about 10^{-3}.

Energetic electrons scattered at the chamber walls contribute a small background to the TPES, proportional to the total ion current. From the analysis of Ar spectra this contribution has been estimated at 0.15% of the total ion current.

C. Total ion scans and photoion–photoelectron coincidences

The 60 V/cm electric field used to extract ions resulted in a constant collection efficiency, independent of fragment ion kinetic energy up to 10 eV. During the total ion scans the extraction field was held constant. However, during the photoion–photoelectron coincidence experiments, threshold electrons were collected in the presence of a 1 V/cm electric field and analyzed as described in the previous section. Ions were then extracted by a −59 V pulse, triggered by the electron signal. The delay between ion formation and the pulse application was approximately 100 nsec, during which time, the ion moved no more than 0.1 mm. Typical ion flight times for NO^+ were 1.2 μsec. The ion scans and TPES were not normalized to the photon flux which

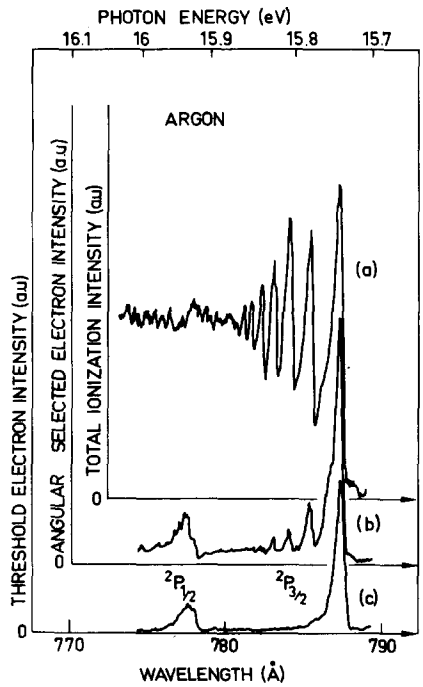

FIG. 4. Threshold photoelectron spectroscopy with time and angular discrimination. (a) Total photoionization spectrum of Ar near its ionization potential obtained with 0.5 Å resolution. (b) TPES of Ar using only angular discrimination of hot electrons. (c) TPES of Ar using both angular and time discrimination with a 4 nsec gate. The intensity scales for (b) and (c) are the same.

varied smoothly and monotonically by about 50% in the wavelength range reported here.

III. RESULTS

A. Photoionization spectra and threshold photoelectron spectra

In Fig. 5, we show the photoionization spectrum and the corresponding TPES in the 970–710 Å (12.7–16.5 eV) region. The previously mentioned autoionizing Rydberg states are clearly evident in the photoionization spectrum. Less obvious is the slow rise in the continuum, especially between 900 and 750 Å. Dashed lines have been drawn to indicate our estimate of the direct ionization continuum and to emphasize the broad feature centered at 840 Å. The latter was first observed by Cook *et al.* [20] and more recently by Berkowitz and Eland. [11b] Cook *et al.* have shown that photoabsorption in the wavelength region under study leads to competition between ionization and dissociation, both on peaks and in valleys of the photoionization spectrum.

In the TPES, the $\tilde{X}\,^2\Pi$ and $\tilde{A}\,^2\Sigma^+$ states of N_2O with resolved vibrational structure are observed. The TPES in the vicinity of the $\tilde{X}$ and $\tilde{A}$ states is similar to the He(I) PES (Fig. 1) except that the intensity of the $\tilde{A}$ state relative to the $\tilde{X}$ state in the TPES is considerably greater, even after the TPES is normalized to the photon intensity. However, the most striking feature in the TPES is the presence of peaks in the gap between the

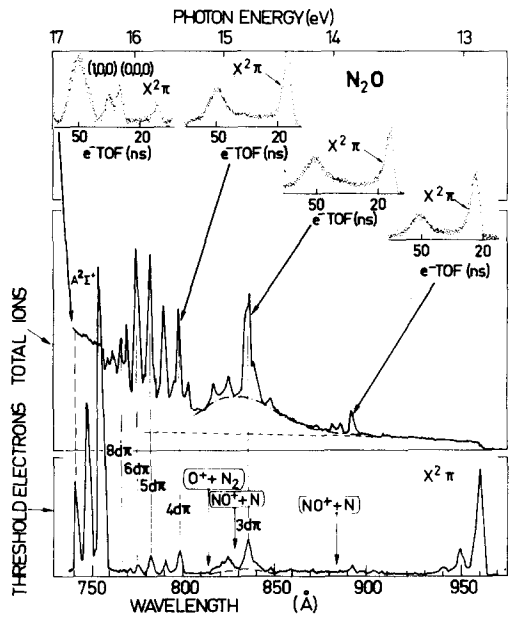

FIG. 5. Total ionization and threshold electron spectra of N_2O as a function of photon energy from the $X\,^2\Pi$ to the $A\,^2\Sigma^+$ states of N_2O^+; the main Rydberg series ($nd\pi$) observed in the TPES are indicated. The first $NO^+ + N$ dissociation limit is indicated at the thermodynamical onset, the second one is the experimental onset of the same fragments. The $O^+ + N_2$ experimental onset occurs at the thermodynamical limit. The dotted curve drawn on the total ion curve is an estimate of the direct ionization continuum of the X state. A broadened group of autoionization states is shown by the dashed lines in the vicinity of 830 Å. On top are four electron time of flight spectra taken at 742, 798, 835, and 893 Å.

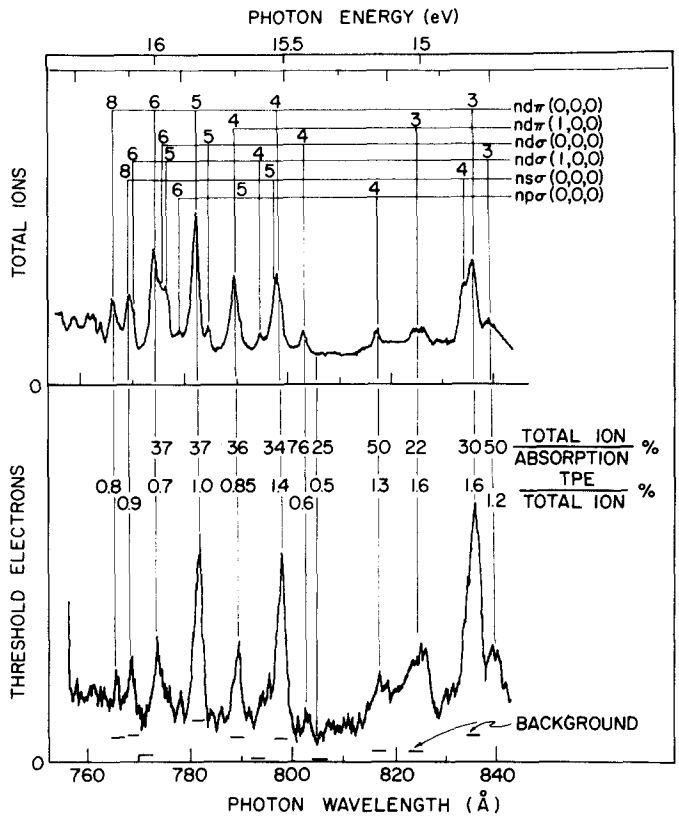

FIG. 6. A higher resolution scan of the ionization efficiency (total ions) and threshold photoelectron spectrum (TPES) between 840 and 760 Å. The Rydberg states are labeled according to Berkowitz and Eland [Ref. 11(b)]. The threshold electron yield (TPE signal/ion signal) and the ionization yield (ionization cross section/absorption cross section) are from Ref. 20.

$\tilde{X}$ and the $\tilde{A}$ states. These peaks correspond to the autoionized states observed in the photoionization spectrum. Figure 6 shows the portion of the spectra dominated by autoionization at a higher resolution.

From the spectra of Figs. 5 and 6, it is possible to calculate the fraction of all the photoelectrons produced in the bandwidth 0–20 meV corresponding to ions of internal energy $h\nu - \text{I. P.}$ This fraction is equal to the (TPES/ION) ratio at each energy divided by the (TPES/ION) ratio at threshold (12.89 eV) where the number of threshold electrons is equal to the number of ions. In doing this, care is taken to subtract the background caused by energetic electrons scattered at the chamber walls, whose magnitude is approximately 0.15% of the ion signal. The results of this analysis for a number of peaks and valleys are shown in Fig. 6. In addition, we have listed selected values of the ionization yield (ratio of the ionization to the absorption cross section) from Ref. 20, and of Rydberg assignments from Ref. 11(b). It is apparent that threshold electrons are detected within the whole wavelength region examined. In particular, the TPE signal does not vanish in the valleys between the autoionization peaks. For the $nd\Pi(0,0,0)$ series one observes a systematic decrease of the TPE yield with increasing principal quantum number. For the other series, systematic trends are less obvious because our resolution is insufficient to resolve overlapping series

and because of the unknown contribution from the underlying continua.

A simple calculation reveals that the fraction of electrons in the 0–20 meV bandpass is remarkably large. Consider the 1.4% for the $4d\Pi$ state at 798 Å which is 2.5 eV above the $\tilde{X}\,^2\Pi(0,0,0)$ state. If the distribution of photoelectron energies were uniform, then each 20 meV interval would receive only 0.8% of the total intensity. Of course, a uniform distribution is not a reasonable assumption. Rydberg states leading to the $\tilde{A}$ state have a geometry similar to the $\tilde{A}$ state: they are linear, as the N_2O^+ $\tilde{X}$ state. Because of the favorable Franck–Condon factors, we expect a considerable fraction of the autoionization to produce N_2O^+ $\tilde{X}\,^2\Pi(0,0,0)$ ions accompanied by the ejection of energetic electrons. These considerations lead inescapably to the conclusion that we have some sort of bimodal distribution of photoelectron energies with energy regions in between of very low probability. One peak must be near 2.5 eV and is associated with the production of ground state N_2O^+ $\tilde{X}$ ions in low vibrational levels, while another peak or set of peaks correspond to low energy electrons which are associated with the production of excited N_2O^+ ions.

In order to supplement the above information and in an attempt to identify the final ion states reached in the various autoionization processes, we measured photoelectron spectra of N_2O at selected wavelengths by the time of flight technique.

B. Photoelectron spectra by electron TOF

Samples of electron TOF spectra are shown in the inserts of Fig. 5. The first spectrum was obtained by exciting N_2O at 774.12 Å the energy of the $A\,^2\Sigma^+$ (2, 0, 0) state of N_2O^+. One observes the (0, 0, 0), (1. 0, 0), and (2. 0, 0) vibrational levels [the latter is not resolved from the (0, 0, 1)] and a peak corresponding to the $X\,^2\Pi$ ground state. The unusual intensity distribution is due to the transmission function of such analyzers which decrease rapidly with energy and thus favors low energy electrons.

The three other electron TOF spectra shown in Fig. 5 were obtained at $\lambda = 798.2$, 835.8, and 891.8 Å, respectively, i.e., on the top of the autoionization peaks, above and below the dissociation limits of N_2O^+. These spectra which are examples of many others obtained on peaks and valleys in the region 755–900 Å all look very similar; they show a large peak corresponding to the formation of N_2O^+ $\tilde{X}\,^2\Pi$ ground state in its low vibrational levels and a second distribution centered at zero energy. The electrons collected within the bandpass 0–20 meV are those responsible for the TPES of the preceding section. Bahr *et al.*[32] also measured photoelectron spectra of N_2O at selected wavelengths in this energy region and observed like us a threshold peak. However, they did not discuss its origin.

For a quantitative interpretation, we have to convert the TOF distributions into energy distributions. This has been done for all the spectra following the procedure outlined in the experimental section II. An example of such a converted spectrum is shown in Fig. 7. The

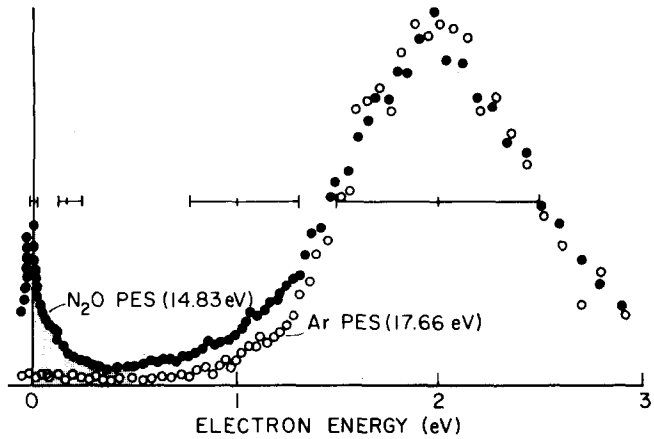

FIG. 7. Photoelectron spectra of N_2O and argon at 1.9 eV above their respective ionization potentials; the horizontal bars indicate the resolution at the nominal energy given by the central point; the shaded region shows the contribution to the N_2O PES between 0 and +500 meV.

incident wavelength for the PES was 835.8 Å (14.83 eV), which is about 1.9 eV above the N_2O ionization potential. For comparison, we have plotted on the same figure the Ar PES obtained at the same energy above its ionization potential. Since the resolution for electrons of 2 eV energy is about 1 eV, neither the spin orbit structure of Ar^+ nor the vibrational levels of N_2O^+ are resolved. The Ar^+ ion has no electronic states 2 eV above its ionization potential other than the $^2P_{1/2}$ and $^2P_{3/2}$ states. Hence, no threshold photoelectrons can be formed at 835.8 Å, and indeed none are observed. Apart from the 2 eV peak, there is just a weak structureless background due to energetic electrons scattered at the chamber walls. In marked contrast, the PES of N_2O exhibits significant electron signal over the whole range of ejection energies, with a sharp peak at zero energy. The resolution near threshold is less than 20 meV, so that the observed 40 meV FWHM of this peak is not limited by instrumental resolution.

The comparison of the Ar and N_2O PES in Fig. 7 shows clearly that the low-energy peak observed in N_2O is not an experimental artifact. The number of TPE collected within the 20 meV bandpass centered at zero energy represents (1.6 ± 0.2)% of all electrons formed (Fig. 6), and the fraction of low energy electrons integrated from 0 to 500 meV (shaded area in Fig. 7) represents about 10% of all electrons. These numbers are, in fact, representative of all N_2O PES obtained both on peaks and in valleys of the photoionization spectrum between the $\tilde{X}$ and $\tilde{A}$ states of N_2O^+. Figure 8 shows examples of PES on an expanded scale, obtained for two peaks and one valley. The Ar PES at the $^2P_{3/2}$ threshold is shown for comparison. The N_2O spectra are normalized to the same total electron count, including the high energy peak not shown in the figure.

It is possible to check that the above spectra are not only qualitatively, but also quantitatively, correct by making use of the photoion–photoelectron coincidence results. These data show that within the experimental uncertainty N_2O^+ is completely predissociated between

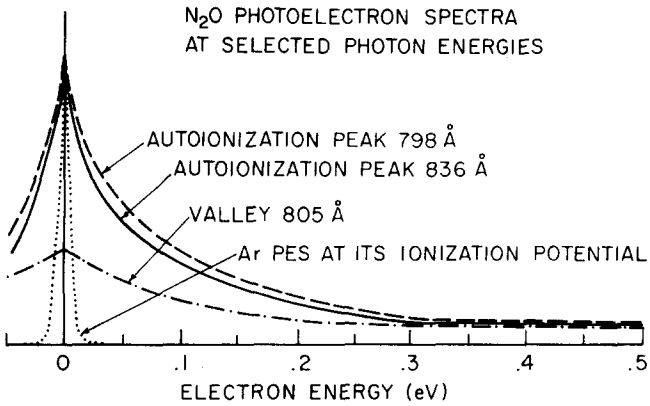

FIG. 8. Selected N_2O PES on peaks and valleys of the photoionization spectrum. The PES of Ar is shown to illustrate the resolution at threshold.

15.0 and 16.0 eV, and that the branching ratio between O^+ and NO^+ is nearly constant at 9 to 1 above the O^+ onset at 15.30 eV. By combining this information with the PES at $\lambda = 798.2$ Å, which represents a plot of the energy deposition function for photoionization at 15.53 eV, we calculate the corresponding ion abundances to be 6% O^+, 3% NO^+, and 91% N_2O^+. These values are in excellent agreement with the 6.4% O^+, 2.6% NO^+, and 91% N_2O^+ obtained directly by photoionization mass spectrometry. [11b]

IV. DISCUSSION

In the following discussion, we first will consider the identification of the N_2O and N_2O^+ states of importance in the region 962–774.1 Å (12.89–16.00 eV) and then the relevant decay mechanisms.

A. Initial states

Photon impact on N_2O in the above energy region can excite three types of states: (1) the ionization continuum of the N_2O^+ $\tilde{X}\,^2\Pi$ ground state; (2) the Rydberg states converging to N_2O^+ $\tilde{A}\,^2\Sigma$ in its low vibrational levels; (3) the dissociation continuum around 840 Å, which is one of a series observed by Cook *et al.* [20] around 840, 740, and 700 Å and which we tentatively assign to Rydbergs converging to the $\tilde{B}\,^2\Pi$ state (18.2 vertical I. P.), the principal effective quantum numbers being 2.0, 3.0, and 5.0, respectively. The recent calculation of Hopper[25] shows the presence of a repulsive $^4A''$ ion state ($^4\Pi$ in the linear conformation) in the relevant energy region. However, this state differs from the neutral ground state by three spin orbitals and has therefore a very small probability of being reached by direct photoionization. For the same reason, the Rydbergs converging to $^4A''$ are unlikely to be formed by photon absorption.

Direct photoionization produces only N_2O^+ $\tilde{X}\,^2\Pi$ in low-vibrational levels, as shown by the He(I) PES (Fig. 1). Our estimate of the importance of this process is indicated by a dashed line in Fig. 5. Franck–Condon factors for the production of vibrationally excited N_2O^+ $\tilde{X}$ levels, on the other hand, are much too small to explain the abundance (~10%) of low-energy electrons some 1 to 3 eV above the I. P. unless the electronic part of the transition matrix element were sharply peaked (~40 meV FWHM) at zero excess energy. As we know of no example of such sharply structured photoionization cross sections, we assume that the low energy electrons observed in the present work are associated with near-resonant *auto*ionization of the Rydbergs mentioned above. We shall now consider the ion states that can be reached by autoionization.

B. Final states

Given our estimate (Fig. 5) for the contribution due to direct ionization into low $\tilde{X}\,^2\Pi$ levels, we find that autoionization accounts for $\gtrsim 80\%$ of the energetic electrons observed in the PES. The relative weight of the low- and high-energy electrons in the PES is thus essentially determined by the relative importance of the corresponding autoionization processes. We find that most of the autoionization (~90%) leads to the formation of N_2O^+ $\tilde{X}\,^2\Pi$ ions in low vibrational levels, as expected from the Franck–Condon factors between the autoionizing Rydbergs converging to $\tilde{A}\,^2\Sigma^+$, and $\tilde{X}\,^2\Pi$, both states being linear with nearly the same equilibrium distances. The ~10% autoionization producing low energy electrons, on the other hand, can produce high vibrational levels of $\tilde{X}\,^2\Pi$, and/or the as yet unobserved $^4A''$. Berkowitz and Eland, [11b] in an attempt to explain the large O^+ and NO^+ signals in the Franck–Condon gap region, suggested that part of the autoionization produces the dissociative $^4A''$. Our results do not support this conclusion. Whether the $^4A''$ state is dissociative or bound, if a significant fraction of the autoionization went to such a state with vertical ionization energy of E_1, our PES would show some peaks or structure at an electron energy of $h\nu - E_1$. The only peak which has a constant $h\nu - E_1$ is the one corresponding to the formation of the $\tilde{X}\,^2\Pi$ in its lowest vibrational levels. The threshold electrons which are observed at all exciting photon energies both below and above the $^4A''$ dissociation limits are therefore not associated with a typical vertical autoionization process into $^4A''$.

In addition, autoionization of Rydbergs converging to $\tilde{A}\,^2\Sigma^+$ into $^4A''$ is very unlikely since the configurations $\cdots (7\sigma)(2\Pi)^4 n\Lambda$ and $\cdots (7\sigma)^2(2\Pi)(\overline{2\Pi})\,3\Pi$ differ by three spin orbitals. From the widths of the autoionization peaks in the spectra of Berkowitz and Eland, [11b] it is evident that the lifetime of Rydbergs such as $3d\Pi$ is at most 10^{-13} sec. The data of Cook *et al.* [20] show that both predissociation and autoionization depopulate these states, and that both decay paths occur at comparable rates. The peak widths observed in the photoionization spectrum therefore give the order of magnitude of the rate of autoionization $\Gamma_a \sim 10^{13}$ sec^{-1}. Given that autoionization yielding low-energy electrons ($\leq$500 meV) competes with that producing energetic electrons in a ratio of about 10 to 1, the rate associated with quasi-resonant autoionization is found to be of the order of 10^{12} sec^{-1}. This value seems much too high to be compatible with the configuration change mentioned above. We conclude that the low-energy electrons are associated with quasiresonant autoionization to $\tilde{X}\,^2\Pi$ in high vibrational levels. At energies in excess of 1 eV above the ground ionic state, the vibrational density of states is

already greater than 2 states/per 10 meV. If we include the rotational states as well, the total density of states is virtually a continuum. Our threshold electron peaks (Figs. 7 and 8) are consistent with this fact in that no structure is evident in the smoothly decreasing signal between 0 and 500 meV electron energy. The production of fragment ions in the Franck–Condon gap will result from the predissociation of the high $\tilde{X}^2\Pi$ levels by the $^4A''$ state. This is a one electron process, probably induced by spin–orbit coupling.

Quasiresonant autoionization into vibrationally excited $\tilde{X}^2\Pi$ is obviously not a "vertical" process. One remains with the question why such a process occurs at a rate as high as 10^{12} sec^{-1}.

C. Autoionization mechanisms

Before commenting on the relevant autoionization mechanisms, we can summarize the main features of these processes as follows: most of the autoionization (90%) leads to N_2O^+ $\tilde{X}^2\Pi$ in low vibrational levels, while quasiresonant autoionization produces $\tilde{X}^2\Pi$ ions with up to 3 eV vibrational energy. The low-energy electrons associated with the latter process show a distribution sharply peaked at zero energy with a width of 40 meV (FWHM), independent of the identity of the autoionized state (n, Λ, v). Furthermore, the threshold photoelectron yield, which essentially reflects the competition between the two autoionization paths, varies only slightly with principal quantum number.

Of these two autoionization paths, the major one can most probably be described and understood within the framework of Fano's CI theory as applied to molecules by Bardsley,[1] Smith,[2,3] and Duzy and Berry.[8] The resonant autoionization process, however, is not consistent with a formulation which only assumes configuration interaction between the Rydberg state and the ionization continuum of the ground state, within the framework of the Born–Oppenheimer approximation, since it does not explain how a large fraction of the electronic energy is transferred to nuclear motion. To use this theory, one would have to invoke an additional intermediate state which could account for high vibrational excitation.

The mechanism for the resonant autoionization is surely a very general one because there is evidence that this process occurs in the autoionization of all polyatomics. The TPES of a number of molecules exhibit peaks in Franck–Condon gap regions.[33,34] The positions of these peaks are correlated with autoionization peaks. In addition, numerous authors[14,16,18,19] have pointed out the fact that fragment ion onsets are observed in Franck–Condon gap regions. The mechanism for producing ions at these energies is certainly the same one which produces the excited N_2O^+ ions reported here.

We have considered a mechanism whereby the autoionized state begins to predissociate towards neutral fragments. If autoionization were to take place in the initial stages of predissociation, a great deal of vibrational energy would remain in the ion due to the stretched bond. An attractive feature of this mechanism is that N_2O is known to be predissociated in the present energy range,[20] and that it would explain how large amounts of energy can be transferred from electronic to vibrational energy. This mechanism is probably a very general one, because competition between autoionization and predissociation occurs in many molecules.[35–37] However, this mechanism does not explain why there should be such a propensity for the ejection of zero energy electrons.

Resonant autoionization may be related to another type of process. The large cross section for ejection of a zero energy electron is remarkably similar to threshold resonances observed in electron scattering of molecules such as HF and HCl.[38] In this process, the excitation cross section peaks whenever the incident electron energy is equal to the vibrational spacing of the target molecule resulting in the ejection of threshold electrons. In both the electron scattering experiment and in autoionization, we have short lived superexcited states. In one case, they are temporary negative ions, in the other, they are autoionizing neutrals. However, the theoretical explanation of these processes is still a matter of debate,[38,39] so that it is uncertain that the physical basis of resonant autoionization and threshold resonances in electron scattering are in any way similar.

V. CONCLUSION

Photoelectron spectra of N_2O obtained by exciting autoionizing Rydberg states below the $\tilde{A}^2\Sigma^+$ state have demonstrated that autoionization in N_2O proceeds via two distinct pathways. The major path (90%) produces N_2O^+ $\tilde{X}^2\Pi$ in low vibrational states as expected on the basis of Franck–Condon factors between the autoionizing Rydberg states and the $\tilde{X}^2\Pi$ state. The remaining 10% of the autoionization results in N_2O ions in the $\tilde{X}^2\Pi$ state with up to 3 eV of vibrational energy. This latter process, termed resonant autoionization is accompanied by the ejection of very low energy electrons in a smoothly varying distribution of energies peaking at zero energy and having a width of about 40 meV.

There is evidence that this autoionization process occurs in many, if not all, polyatomic molecules; it would thus explain the observation of fragmentions onsets in Franck–Condon gap regions.

ACKNOWLEDGMENTS

We are grateful for helpful discussions with Professor J. Durup. We would like to thank Dr. P. Marin and his colleagues of the linear accelerator for their help and support. Finally, Tomas Baer thanks the Guggenheim foundation for a fellowship and the National Science Foundation for partial support of this work.

[1] J. N. Bardsley, Chem. Phys. Lett. **1**, 229 (1967); **2**, 329 (1968).
[2] A. L. Smith, Philos. Trans. R. Soc. London Sect. A **268**, 169 (1970).
[3] A. L. Smith, J. Quant. Spectrosc. Radiat. Transfer **10**, 1129 (1970).
[4] U. Fano, Phys. Rev. **124**, 1866 (1961).

[5]U. Fano and J. W. Cooper, Phys. Rev. Sect. A **137,** 1364 (1965).
[6]J. A. Kinsinger and J. W. Taylor, Int. J. Mass. Spectrom. Ion Phys. **11,** 461 (1973).
[7]J. Berkowitz and W. A. Chupka, J. Chem. Phys. **51,** 2341 (1669).
[8]C. Duzy and R. S. Berry, J. Chem. Phys. **64,** 2431 (1976).
[9](a) A. J. Blake, J. L. Bahr, J. H. Carver, and V. Kumar, Philos. Trans. R. Soc. London Sect. A **268,** 169 (1970); (b) J. L. Bahr, A. J. Blake, J. H. Carver, J. L. Gardener, and V. Kumar, J. Quant. Spectrosc. Radiat. Transfer **11,** 1839 (1971); **12,** 59 (1972); (c) J. H. Carver and J. L. Gardener, J. Quant. Spectr. Radiat. Transfer **12,** 207 (1972).
[10]T. Baer and B. P. Tsai, J. Electron Spectr. **2,** 25 (1973).
[11](a) V. H. Dibeler, J. A. Walter, and S. K. Liston, J. Res. Natl. Bur. Stand. A **71,** 371 (1967); (b) J. Berkowitz and J. H. D. Eland, J. Chem. Phys. **67,** 2740 (1977).
[12](a) K. E. McCulloh, J. Chem. Phys. **59,** 4250 (1973); (b) J. H. D. Eland and J. Berkowitz, J. Chem. Phys. **67,** 2782 (1977).
[13]V. H. Dibeler and S. K. Liston, J. Chem. Phys. **49,** 482 (1968).
[14]P. M. Guyon, W. A. Chupka, and J. Berkowitz, J. Chem. Phys. **64,** 1419 (1976).
[15]A. C. Parr and F. A. Elder, J. Chem. Phys. **49,** 2659 (1968).
[16]A. C. Parr, A. J. Jason, and R. Stockbauer, Int. J. Mass. Spectrom. Ion Phys. **26,** 23 (1978).
[17](a) D. W. Turner, C. Baker, A. D. Baker, and C. R. Brundle, *Molecular Photoelectron Spectroscopy* (Wiley-Interscience, London, 1970); (b) R. Frey, B. Gotchev, W. B. Peatman, H. Pollack, and E. W. Schlag, Chem. Phys. Lett. **54,** 411 (1978).
[18]H. M. Rosenstock, K. E. McCulloh, and F. P. Lossing, Int. J. Mass Spectrom. Ion Phys. **29,** 327 (1977).
[19]W. A. Chupka, in *Chemical Spectroscopy and Photochemistry in the Vacuum Ultraviolet,* edited by C. Sandorfy, P. J. Ausloos, and M. B. Robin (Reidel, Boston, 1974).
[20]G. R. Cook, P. H. Metzger, and H. Ogawa, J. Opt. Soc. Am. **58,** 129 (1967).
[21]Y. Tanaka, A. S. Jursa, and F. J. LeBlanc, J. Chem. Phys. **32,** 1205 (1960).
[22](a) J. H. D. Eland, Int. J. Mass Spectrom. Ion Phys. **12,** 389 (1973); (b) B. Brehm, R. Frey, A. Kustler, and J. H. D. Eland, Int. J. Mass Spectrom. Ion Phys. **13,** 251 (1974).
[23](a) E. H. Fink and K. H. Welge, Z. Naturforsch. Teil A **23,** 358 (1968); (b) W. H. Smith, J. Chem. Phys. **51,** 3410 (1969); (c) J. H. D. Eland, M. Devoret, and S. Leach, Chem. Phys. Lett. **43,** 97 (1976); (d) J. Maier (private communication); (e) R. Frey, B. Gotchev, W. B. Peatman, H. Pollak, and E. W. Schlag, Chem. Phys. Lett. **54,** 411 (1978).
[24]R. G. Orth and R. C. Dunbar, J. Chem. Phys. **66,** 1616 (1977).
[25](a) D. G. Hopper, Chem. Phys. Lett. **31,** 446 (1975); (b) D. G. Hopper, J. Am. Chem. Soc. **100,** 1019 (1978).
[26]P. M. Guyon, T. Baer, L. F. A. Ferreira, I. Nenner, A. Tabche-Fouhaille, R. Botter, and T. Govers, J. Phys. B **11,** L141 (1978).
[27]P. M. Guyon, C. Depautex, and G. Morel, Rev. Sci. Instrum. **47,** 1347 (1976).
[28]W. C. Wiley and I. H. McLaren, Rev. Sci. Instrum. **26,** 1156 (1955).
[29]B. P. Tsai, T. Baer, and M. L. Horowitz, Rev. Sci. Instrum. **45,** 494 (1974).
[30](a) T. Baer, W. B. Peatman, and E. W. Schlag, Chem. Phys. Lett. **4,** 243 (1969); (b) R. Spohr, P. M. Guyon, W. A. Chupka, and J. Berkowitz, Rev. Sci. Instrum. **42,** 1872 (1971).
[31](a) T. Baer, B. P. Tsai, D. Smith, and P. T. Murray, J. Chem. Phys. **64,** 2460 (1976); (b) C. F. Batten, J. A. Taylor, and G. G. Meisels, J. Chem. Phys. **65,** 3316 (1976); (c) R. Frey, B. Gotchev, O. F. Kalman, W. B. Peatman, H. Polak, and E. W. Schlag, Chem. Phys. **21,** 89 (1977); (d) R. Stockbauer, Int. J. Mass Spectrom. Ion Phys. **25,** 89 (1977).
[32]J. L. Bahr, J. Blake, J. H. Carver, J. L. Gardner, and V. Kumar, J. Quant. Spectrom. Rad. Transfer **12,** 59 (1972).
[33]P. T. Murray and T. Baer, Int. J. Mass Spectrom. Ion Phys. (in press).
[34]V. K. Potapov, G. V. Karachevtsev, and M. M. Lipei, Khim. Vysokikh Energii **11,** 107 (1977).
[35]R. L. Platzman, J. Phys. Radium (Paris) **21,** 853 (1960).
[36]W. P. Jesse and R. L. Platzman, Nature (London) **195,** 790 (1962).
[37]G. V. Marr, *Photoionization Processes in Gases* (Academic, New York, 1967).
[38]K. Rohr and F. Linder, J. Phys. B **9,** 2521 (1976).
[39]L. Dubé and A. Herzenberg, Phys. Rev. Lett. **38,** 820 (1977).